Ligand-Effect-Induced Oxygen Reduction Reaction Activity Enhancement for Pt/Zr/Pt(111) Surfaces with Tensile Strain Relieved by Stacking Faults

doi: 10.1021/acsaem.9b00873

Ligand-effect-induced Oxygen Reduction Reaction Activity Enhancement for Pt/Zr/Pt(111) Surfaces with Tensile Strain Relieved by Stacking Faults

Daisuke Kudo[1], *Soma Kaneko*[1], *Rikiya Myochi*[1], *Yoshihiro Chida*[1], *Naoto Todoroki*[1*], *Tadao Tanabe*[2], *Toshimasa Wadayama*[1]

[1] Graduate School of Environmental Studies, Tohoku University, Sendai 980-8579, Japan

[2] Graduate School of Engineering, Tohoku University, Sendai 980-8579, Japan

KEYWORDS: oxygen reduction reaction; Pt-shell; tensile strain; Pt–Zr surface alloy; stacking fault; arc-plasma deposition; in-plane XRD, cross-sectional STEM

ABSTRACT

Oxygen reduction reaction (ORR) properties are investigated for the Pt/Zr/Pt(111) surfaces prepared through arc-plasma-depositions of Zr and Pt on Pt(111) substrate. The synthesized Pt(111)-shell surfaces on Pt-Zr(111) alloy layers exhibited 3 to 5-fold higher ORR activities than the clean Pt(111): the ligand effect is deduced for the enhanced activities through charge-transfers between the surface Pt and Zr atoms, though tensile strains relieved by the stacking faults worked

on the Pt(111)-shells. Furthermore, the alloy surfaces are durable against an electrochemical potential cycling. The results demonstrate that Zr should be considered for alloying elements of Pt for developments of effective ORR catalysts.

INTRODUCTION

Proton-exchange membrane fuel cells (PEMFCs) are vital energy-conversion devices in a hydrogen-fueled society.[1] A number of papers for the Pt and Pt-based alloys have been published subjected to synthesize highly-active electrode materials to promote the rather slow kinetics of the electrochemical oxygen reduction reaction (ORR).[2-4] The near-surface nano-structures of Pt-based alloy nano-particles with a Pt-shell and a noble or noble-less metal-element core are one of the keys for developing superior cathode catalysts for PEMFCs.[5] The fore-mentioned studies clearly exhibit that strain (geometric) and ligand (electronic) effects on the Pt shells, which are essential for enhancing the mass-activity of Pt.[6-7] In other words, the ORR activity enhancement depends on the atomic arrangements of the topmost surface of the Pt shells, and on the alloy compositions of the underlying alloy cores.[8] Because the compressively strained Pt-shell is known to be a key factor for the activity enhancements, exploring of alloying core-metals are focused on smaller atomic radius of group 9 to 11 late transition metals, e.g., Ni, Co, Pd, Ir, Cu, etc, relative to Pt[9] . Indeed, Čolić et al. summarized the published ORR activity trends of various Pt-based alloys as a function of atomic radius of alloying metals,[10] in which the highest ORR activities of the Pt-Cu and Pt-Y showed “double volcano” and the activities of the alloys for early transition metals, e.g. Ti, Hf, Zr etc. were much lower. On the other hand, the group 4 early transition metal elements such as Zr are corrosion-resistant in the operating environments of PEMFCs (e.g., pH = 1)[11] and,

thereby, alloying element of Ze should improve the durability of the alloy catalyst. However, to date, the ORR performances of Pt–Zr alloys have been rarely studied[12]. Larger atomic radii of such the early transition metals generally induce a not compressive- but tensile-strain of the surface Pt-shell layers. As a result, correlations of the tensile-strain-induced Pt shells and the ORR performances (activity and durability) remained to be investigated experimentally.

By engineering the strain on well-defined Pt-based single-crystal alloy surfaces, we can discuss the ORR activity and durability enhancement mechanisms of catalysts synthesized with precisely-controlled nano-architectures.[13-14] Previously, we published the electrochemical properties of arc-plasma deposited (APD) Pt-based alloy model catalysts, and related their ORR activities to their nano-structures.[15-17] In this study, we synthesize hetero-layered Pt and Zr nano-structures on surface-cleaned Pt(111) substrate as a model of PEMFC cathode catalysts. The Pt and Zr were alternately deposited by the APD method in ultra-high vacuum (UHV; ~10^{-8} Pa). The ORR activities of the synthesized Pt(111)-shell layers with tensile strains (less than 0.8 %) on the face centered cubic (fcc) Pt–Zr(111) alloy layers were 3- to 5-fold higher than those of clean Pt(111). Furthermore, the resulting Pt(111)-shell surfaces were electrochemically stable under potential cycling of 0.6 and 1.0 V vs RHE. The results demonstrate that alongside the Group 9–11 late transition metal elements (such as Ni, Co, and Pd), alloy systems of Pt and early transition metals, e.g., Zr are potentially suitable materials for cathode electrodes.

EXPERIMENTAL

The experimental apparatus used in this study is described elsewhere.[13, 15-16] The Pt(111) (< 0.1° miscut) crystal surface was cleaned by repeated Ar^+ sputtering and annealing at 1153 K under UHV conditions. The Zr and Pt layers were alternately deposited onto the clean Pt(111) substrate

by two APD sources (ULVAC-RIKO ARL-300), also under UHV conditions. The deposition sequences and conditions are summarized in Figure S2 and Table S1 of the Supporting Information (SI). The total thicknesses of the Pt, first-layer Zr, and fourth-layer Pt (shell) were fixed at 6.0 nm, 0.4 nm, and 1.6 nm, respectively, and the combined thickness of the second-layer Pt and third-layer Zr (beneath the shell) was 4.0 nm. The thickness of the third-layer Zr was varied as 0.4, 0.8, 1.6, and 3.2 nm, and the resulting Pt/Zr/Pt(111) alloy surfaces were denoted as U_Zr0.4nm, U_Zr0.8nm, U_Zr1.6nm, and U_Zr3.2nm, respectively. The surface nano-structures of the APD-synthesized Pt/Zr/Pt(111) surfaces were investigated by in-plane XRD (Rigaku, Smart Lab) in air, and by cross-sectional high-angle annular dark-field scanning transmission electron microscopy (HAADF-STEM) combined with energy-dispersive X-ray spectrometry (EDS) (JEOL, JEM-ARM200F). For the electrochemical measurements, the Pt/Zr/Pt(111) surfaces were transferred to a N_2-purged glove-box (1 atm) in a transfer vessel[18] to avoid possible surface oxidation. The cyclic voltammograms (CV; scan rate = 50 mV s^{-1} without disk rotation) and linear sweep voltammograms (LSV; scan rate = 10 mV s^{-1}) were recorded in N_2-purged and O_2-saturated 0.1M $HClO_4$ (Ultrapure, Kanto Chemical) in the glove-box. All potentials described have been presented with respect to RHE.

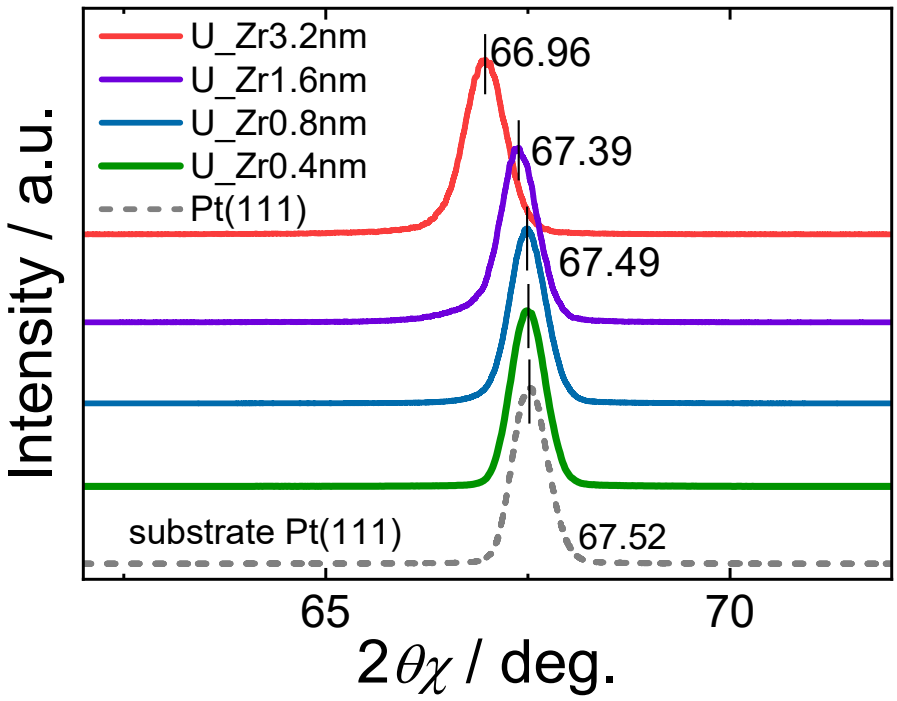

Figure 1. in-plane XRD patterns of the Pt/Zr/Pt(111) surfaces in the region of (220) of the Pt(111) substrate (67.52°). The X-ray incident angle is 0.1°.

RESULTS AND DISCUSSIONS

The in-plane XRD patterns of the Pt/Zr/Pt(111) surfaces were obtained under Cu Kα radiation (λ = 0.1542 nm) at $2\theta\chi$ angles ranging from 62° to 72°. The results are presented in Figure 1. The detection layout of the diffracted X-rays, and a zoom-in of the XRD patterns in the 65–69° range, are schematized in Figure S3 of SI. Because the in-plane XRD patterns provide the distances of the lattice planes oriented normal to the Pt(111) substrate, the lattice distance in the (220) diffraction plane of the Pt(111) substrate should provide the surface strain of the Pt(111) shells on the substrate. The in-plane XRD peaks of Pt(220) clearly shifted to lower diffraction angles with increasing deposition thickness of the third-layer Zr. The surface strains ($\varepsilon_{Pt(111)\text{-}shell}$ (%)) in the

Pt(111) shells were estimated from the difference between the lattice parameter *d* in the <220> direction of the surface Pt(111) shell and the *d* of the substrate Pt(111):

$$\epsilon_{Pt(111)-shel}\ (\%) = \frac{d_{Pt(111)-shel} - d_{Pt(111)substrate}}{d_{Pt(111)substrate}} \times 100 \quad (1)$$

where $d_{Pt(111)\text{-}shell}$ and $d_{Pt(111)substrate}$ were estimated from the measured diffraction angles of Pt(220) under the Bragg condition $2d\sin\theta = n\lambda$.

Table 1 lists the estimated $\varepsilon_{Pt(111)\text{-}shell}$ (%) of the synthesized Pt/Zr/Pt(111) surfaces. The alternate depositions of Zr and Pt on the Pt(111) substrate induced tensile strains in the Pt(111)-shell lattices, probably because the atomic radius of Zr is approximately 15 % larger than that of Pt. One might notice that the estimated strains are smaller than the compressive strains in APD-synthesized Pt/Co/Pt(111) (up to 3.2% vs. Pt(111)).[13] The XPS spectra of the as-synthesized, pristine U_Zr3.2nm (Figure S7 in SI) showed the deconvoluted Pt4$f_{7/2}$ band centered at 71.35 eV that ascribable to the metallic state of Pt (Pt^0). The binding energy of Pt^0 band was positively shifted by ca. 0.15 eV from the clean Pt(111), suggesting that electronic charge transfer between Pt and Zr.

Table 1. Tensile strains on the Pt(111)-shell surfaces, estimated from the in-plane XRD results

	U_Zr0.4nm	U_Zr0.8nm	U_Zr1.6nm	U_Zr3.2nm
$\varepsilon_{Pt(111)\text{-}shell}$ (%)	<+0.04	+0.05	+0.20	+0.75

Figure 2 shows the cross-sectional HAADF-STEM images of U_Zr3.2nm collected from the <110> direction (the (110) cross-section). The regions enclosed within the white squares of the left-hand image are magnified in the corresponding panels on the right. Typical EDS line profiles of the Pt (black) and Zr (orange) in U_Zr3.2nm are also shown. Judging from the broad Z-contrast at approximately 2 nm from the top surface of U_Zr3.2nm, the atomic near-surface structure was composed not of abrupt alternating layers of Pt and Zr (super lattice), but of Pt–Zr surface alloys. Furthermore, in both samples, the stacking sequence of the (111) planes was A, B, C, revealing an fcc-dominated lattice structure. From the Pt–Zr phase diagram (Figure S1 in SI), the solid-solution limit of Zr and Pt (which also has an fcc structure) was estimated as ca. 20 at%, and the substrate temperature of APD (873 K; see SI) was too low to generate intermetallic alloy compounds such as $ZrPt_3$, ZrPt, and Zr_5Pt_3. Indeed, the Zr composition in the 2 nm-thick regions under the Pt(111)-shell was estimated to be 17 at%, which is lower than the solid-solution limit (Figure S4 in SI). Furthermore, in the EDS line profiles of Pt and Zr in Fig. 2, the Pt signal increased from the topmost surface and the Zr signal becomes obvious at ca. 0.5–5.0 nm from the top surface. These results are consistent with the formation of a ca. 0.5 nm-thick Pt(111) shell on the ca. 4 nm-thick Pt–Zr(111) surface alloy with an fcc structure, confirming that such a structure can be synthesized by the APD sequence. Several stacking faults are visible in the STEM images. For example, in region (i) of Fig. 2, the (111) stacking sequence changes from A, B, C to C, B, A at ca. 10 stacking layers from the top-surface, forming a twin boundary (vertical dashed line). Furthermore, as shown in the magnified image of region (iii), twin boundaries were generated at 7 and 10 stacking layers from the top-surface, accompanying the coherent A, B, C stacking in region (ii). As mentioned above, the estimated tensile strains in the Pt(111)-shells were smaller than the compressive strains in the Pt(111)-shells coherently grown on Pt-Co(111) alloy layers.[13] The stacking faults shown in

Figure 2 are known to relieve the elastic strain in epitaxial systems,[19] so the rather small tensile strains on the Pt/Zr/Pt(111) surfaces (less than 1% that of clean Pt(111)) can be explained by the generated stacking faults (twinning).

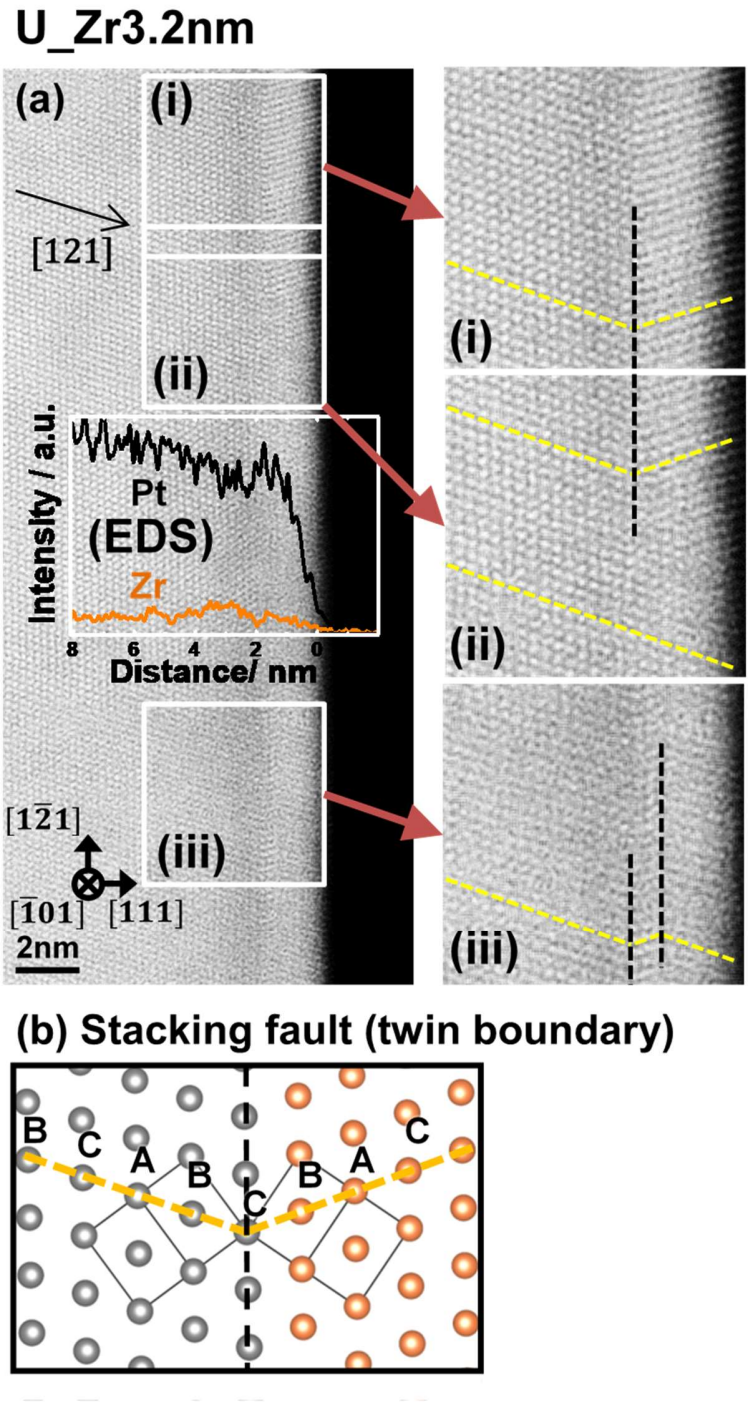

Figure 2. (a) Cross-sectional STEM image of U_Zr3.2nm. The right-side panels are magnifications of the corresponding regions enclosed in the white squares ((i)–(iii)) at the left

Typical EDS line profiles of Pt (black) and Zr (orange) are shown on the central-left image. (b) Atomic model of the twin boundary in the (110) cross-section.

The CV curves of the Pt/Zr/Pt(111) surfaces are presented in Figure 3. For a reference, a CV of the clean Pt(111) (dashed line) is also depicted in each CVs. The hydrogen adsorption charge (Q_H) decreased at lower shifts of the onset potentials of hydrogen adsorption (negative potential scan), consistent with previous reports on well-defined Pt(111)-shell surfaces with high ORR activity.[20-21] Furthermore, the Q_H and the onset potential shifts on the compressively-strained Pt/Co/Pt(111) surfaces decreased with increasing thickness of the underlying Co deposition.[13] In contrast, the afore-mentioned Pt/Zr/Pt(111) surfaces were insensitive to thickness of the underlying Zr deposition. The positive shifts of the onset potentials are attributable to change in adsorption behaviors of hydroxyl-related (OH) species (ca. 0.6 V; positive potential scan), while the so-called butterfly peak (appearing at 0.8 V in clean Pt(111)) shifted only slightly (Figure S5 in SI). The CVs in Figure 3 clearly showed that the electrochemical properties of the Pt(111)-shell surfaces were effectively modified by charge transfers between Pt-shells and the underlying Zr (Pt-Zr) atoms.

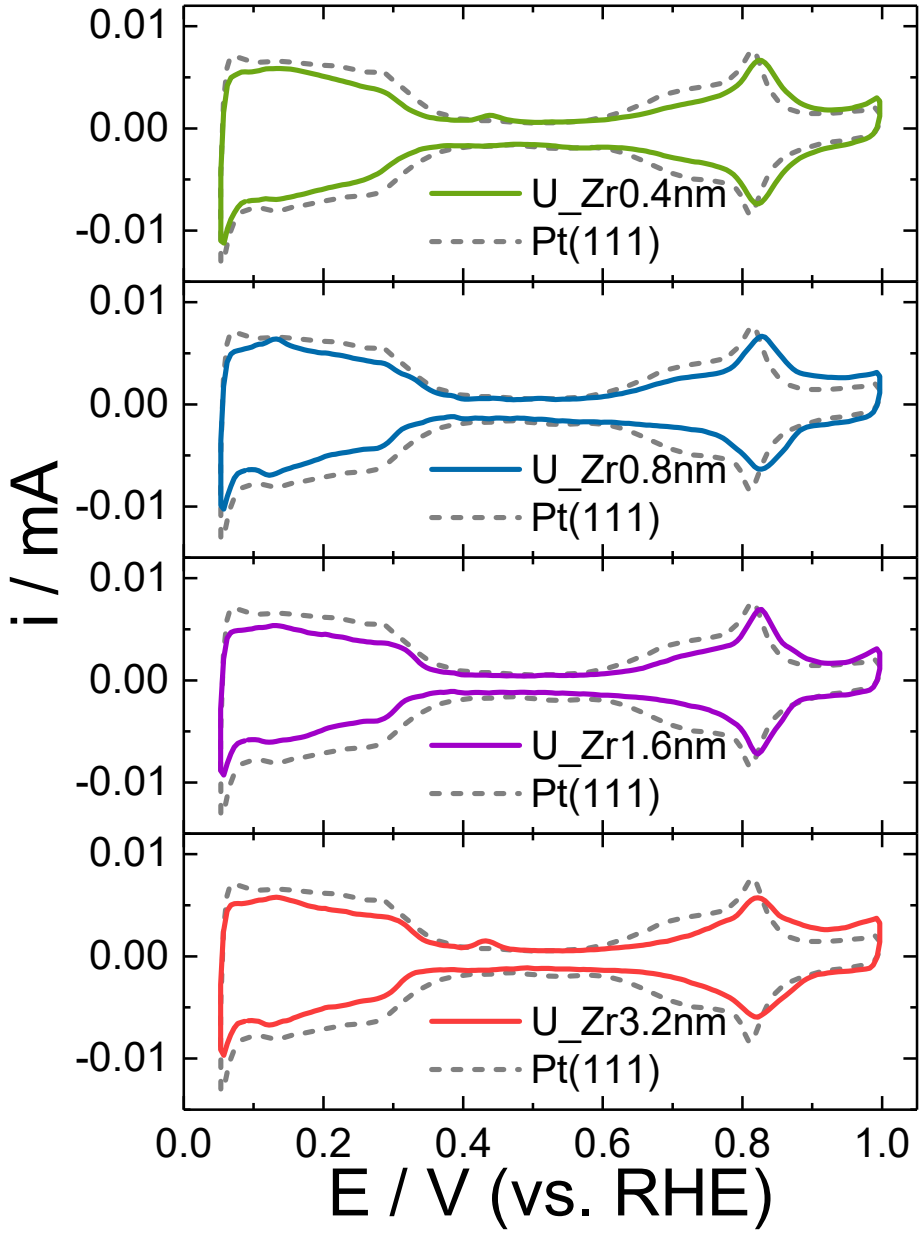

Figure 3. CV curves of the Pt/Zr/Pt(111) surfaces recorded in N_2-purged 0.1 M $HClO_4$.

The LSV curves of Pt/Zr/Pt(111) in the O_2-saturated 0.1 M $HClO_4$ and their corresponding Tafel plots are summarized in Figure S6 of the SI. The half-wave potentials in each LSV curve were positively shifted relative to clean Pt(111), indicating the enhanced ORR activity of Pt/Zr/Pt(111). The ORR activity was judged from the limited current density (j_k) at 0.9 V, estimated by the Koutecky–Levich equation. Figure 4 shows the initial activity enhancement factors and the corresponding tensile strains of the Pt/Zr/Pt(111) surfaces (estimated from the in-plane XRD patterns), as functions of deposition thicknesses of the third-layer Zr. The enhancement factors for the Pt/Zr/Pt(111) surfaces are 3 – 5 times higher than the clean Pt(111): ca. 0.05 % tensile-strained U_Zr0.8nm exhibits a maximum enhancement factor of 5. In compressive-strained Pt(111)-shell surfaces, the ORR vs. strain curve exhibits a volcano-type trend, with the maximum activity observed in ca. 2% compressively strained surface.[13, 22] In contrast, correlation between estimated ORR activities and tensile strains were indistinct for the Pt/Zr/Pt(111) surfaces.

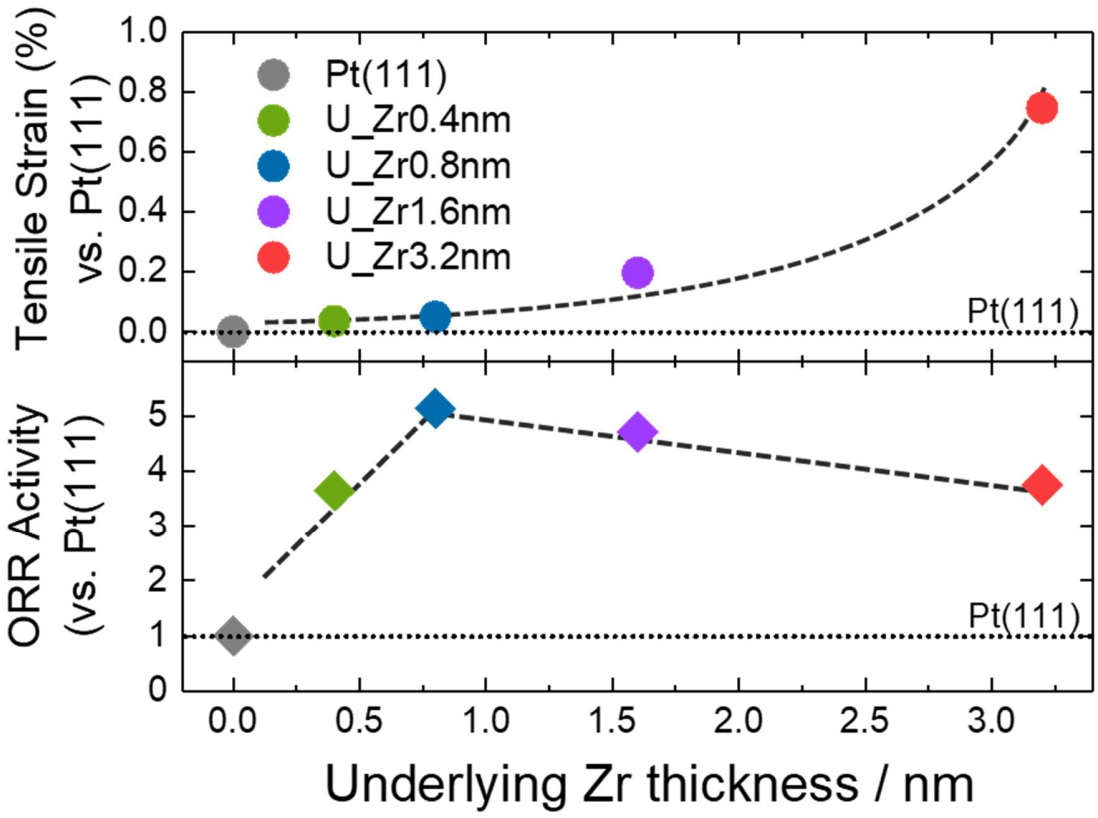

Figure 4. ORR activity enhancement factors (bottom) and tensile strains vs. deposition thickness of the third-layer Zr (underlying Pt-shell).

The ORR activity enhancement of the Pt-based alloys can be explained by decrease in adsorption energy for the oxygen-related species and/or d-band center shifts of Pt by the alloying.[23] The Pt-shell surfaces might be electronically modified by charge transfers between Pt and the adjacent alloying elements M (the ligand effect).[24] Also, compressive strains worked on the Pt(111)-shells lead to decrease in the adsorption energy of the oxygen-related species (strain effect).[25-26] To our knowledge, tensile strains on the surfaces of the Pt(111) shells are negative for ORR activity enhancement[27]. The ORR enhancement mechanism (ligand or strain effect) can be

distinguished by the locations of the M atoms. In the former ligand effect, the M atoms are required to site neighboring of the top-surface Pt atoms. In this study, the deposition thickness of the fourth-layer Pt (shell) was fixed at 1.6 nm, and the actual Pt(111)-shell thickness was estimated as ca. 0.5 nm from the EDS line profiles of U_Zr3.2nm (Figure 2). Actually, the STEM-EDS analysis showed that Zr composition in the Pt-Zr alloy layers under the Pt(111)-shell can be estimated to be 17 at% (Figure S4 in SI) shows, suggesting the Zr atoms adjacent to the Pt-shell should be present. Therefore, we deduce from the fore-mentioned discussions that the charge-transfer between surface Pt and neighbouring Zr atoms dominantly contribute to the ORR activity enhancements for the synthesized Pt/Zr/Pt(111) surfaces, though in-plane tensile strains relieved by the stacking faults worked on the surface Pt(111) lattices.

Figure 5 shows the ORR activity trends of the Pt/Zr/Pt(111) surfaces under potential cycles (PCs) of 0.6 and 1.0 V vs. RHE (inset) in oxygen-saturated 0.1 M $HClO_4$. The ORR was substantially deactivated for all the surfaces in the earliest PCs (fewer than 100 PCs), particularly for U_Zr0.8nm and U_Zr1.6nm. The results suggest that the Zr atoms located at very near surface region could be passivated to ZrO_x even at earliest PCs. As a result, the ligand effect for ORR enhancement of the Pt(111)-shell that induced by the adjacent Zr atoms seems to be lowered. At any rate, although passivation of the surface Zr atoms by the PCs should determine deactivation behaviors, initial Pt/Zr alloy compositions at near surface regions cannot be determined at present and, thus, no further discussions have been made in this study. After the 100 PCs, the sample surfaces were stabilized by the surface ZrO_x and, then, the U_Zr1.6nm sustained its ~3-fold activity (relative to pristine clean Pt(111)) even after 5000 PCs. Moreover, the Zr 3*d* XPS band of pristine U_Zr3.2nm remained nearly unchanged after 5000 PCs (Figure S7 in SI), suggesting that the passivated Zr in the near-surface regions remained stable during the PCs. Previously, we

investigated the structural stabilities of various well-defined Pt–M(111) surfaces (M = Ni, Co, Pd, and others) under the same potential cycling protocol.[28-30] As a comparative example, the XPS band intensities of Ni 2*p* on the bimetallic surfaces of 4 monolayer-thick Pt(111)/Pt_xNi_{100-x}(111) (x = 75, 50, 25) increased after 1000 PCs for x = 75 and 50, and decreased for x = 25.[21] Such changes in the Ni band intensity were attributed to the dynamic behaviors of the Ni alloying element (i.e., inter-diffusions of Ni atoms in the surface regions). As the PCs continued, the dissolved Ni atoms altered the Pt-shell structures. Although the mechanism of durability enhancement needs clarifying by atomically-resolved surface observations, the results confirm the durability of the Pt–Zr alloy surfaces under the PEMFC operating conditions.

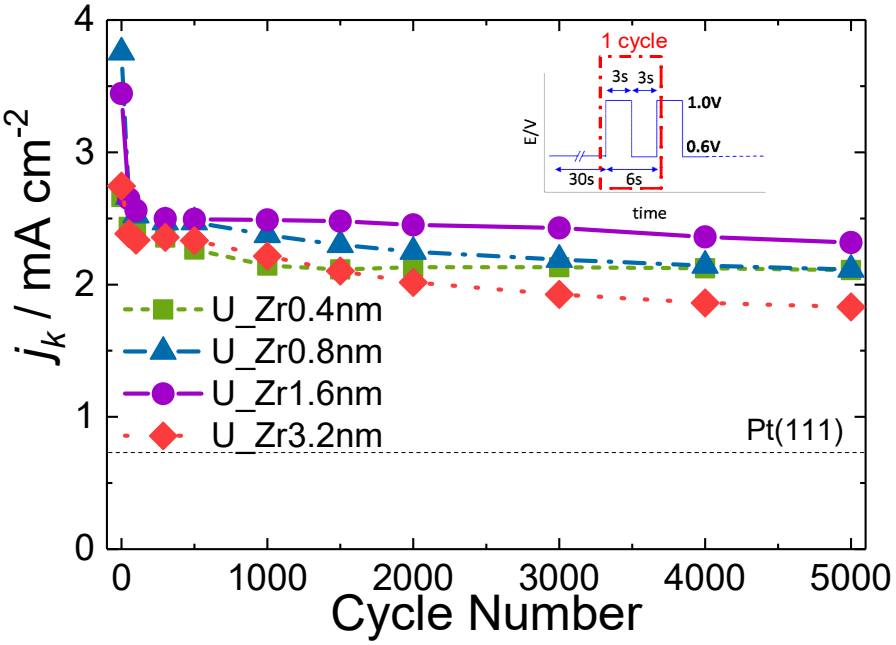

Figure 5. ORR activity trends of the Pt–Zr(111) surfaces under potential cycles of 0.6 and 1.0 V vs. RHE (inset) in oxygen-saturated 0.1 M $HClO_4$.

SUMMARY

In summary, we synthesized the Pt/Zr/Pt(111) surfaces that comprised of the Pt(111)-shells on Pt-Zr(111) alloy layers by alternative APDs of Zr and Pt on the clean Pt(111) in UHV. Judging from the in-plane XRD diffraction peaks of Pt(220), small tensile strains (less than 0.8% on average) acted on the Pt(111)-shell surfaces, while local microstructures, such as stacking faults in fcc(111), were generated in the Pt(111) shells, around the interface region of the shells, and in the underlying Pt–Zr(111) alloy layers. The synthesized Pt(111) shell surfaces achieved a 3–5 fold higher ORR activity than Pt(111) and high durability against PCs. The results demonstrate that Zr, a group 4 early transition metal, should be considered as for the alloying element of Pt to develop high-performance cathode catalysts of the PEMFCs.

ASSOCIATED CONTENT

Supporting Information

The Supporting Information is available free of charge on the ACS Publications website at DOI: Included are a phase diagram of Pt-Zr, detailed APD sequences and conditions, enlarged in-plane XRD patterns, a STEM-EDS analysis for the U_Zr3.2nm, enlarged CVs in the potential region of OH adsorption, LSVs recorded in O_2-saturated 0.1M $HClO_4$, Tafel plots, and XP spectra recorded before and after the 5000 PCs.

AUTHOR INFORMATION

Corresponding Author

* E-mail: n-todoroki@material.tohoku.ac.jp

ACKNOWLEDGMENTS

This study was supported by the New Energy and Industrial Technology Development Organization (NEDO) of Japan.

REFERENCES

(1) Yu, Y.; Li, H.; Wang, H.; Yuan, X.-Z.; Wang, G.; Pan, M. A Review on Performance Degradation of Proton Exchange Membrane Fuel Cells During Startup and Shutdown Processes: Causes, Consequences, and Mitigation Strategies. *J. Power Sources* 2012, 205, 10-23.
(2) Bu, L.; Zhang, N.; Guo, S.; Zhang, X.; Li, J.; Yao, J.; Wu, T.; Lu, G.; Ma, J.-Y.; Su, D.; Huang, X. Biaxially Strained Ptpb/Pt Core/Shell Nanoplate Boosts Oxygen Reduction Catalysis. *Science* 2016, 354, 1410-1414.
(3) Hwang, S. J.; Kim, S.-K.; Lee, J.-G.; Lee, S.-C.; Jang, J. H.; Kim, P.; Lim, T.-H.; Sung, Y.-E.; Yoo, S. J. Role of Electronic Perturbation in Stability and Activity of Pt-Based Alloy Nanocatalysts for Oxygen Reduction. *J. Am. Chem. Soc.* 2012, 134, 19508-19511.
(4) Escudero-Escribano, M.; Malacrida, P.; Hansen, M. H.; Vej-Hansen, U. G.; Velázquez-Palenzuela, A.; Tripkovic, V.; Schiøtz, J.; Rossmeisl, J.; Stephens, I. E. L.; Chorkendorff, I. Tuning the Activity of Pt Alloy Electrocatalysts by Means of the Lanthanide Contraction. *Science* 2016, 352, 73-76.
(5) Liu, M.; Zhao, Z.; Duan, X.; Huang, Y. Nanoscale Structure Design for High-Performance Pt-Based Orr Catalysts. *Adv. Mater.* 2019, 31, 18022341-18022348.
(6) Jia, Q.; Caldwell, K.; Strickland, K.; Ziegelbauer, J. M.; Liu, Z.; Yu, Z.; Ramaker, D. E.; Mukerjee, S. Improved Oxygen Reduction Activity and Durability of Dealloyed Ptcox Catalysts for Proton Exchange Membrane Fuel Cells: Strain, Ligand, and Particle Size Effects. *ACS Catal.* 2015, 5, 176-186.
(7) Fako, E.; Dobrota, A. S.; Pašti, I. A.; López, N.; Mentus, S. V.; Skorodumova, N. V. Lattice Mismatch as the Descriptor of Segregation, Stability and Reactivity of Supported Thin Catalyst Films. *Phys. Chem. Chem. Phys.* 2018, 20, 1524-1530.
(8) Suen, N.-T.; Hung, S.-F.; Quan, Q.; Zhang, N.; Xu, Y.-J.; Chen, H. M. Electrocatalysis for the Oxygen Evolution Reaction: Recent Development and Future Perspectives. *Chem. Soc. Rev.* 2017, 46, 337-365.
(9) Kulkarni, A.; Siahrostami, S.; Patel, A.; Norskov, J. K. Understanding Catalytic Activity Trends in the Oxygen Reduction Reaction. *Chem. Rev.* 2018, 118, 2302-2312.
(10) Čolić, V.; Bandarenka, A. S. Pt Alloy Electrocatalysts for the Oxygen Reduction Reaction: From Model Surfaces to Nanostructured Systems. *ACS Catal.* 2016, 5378-5385.
(11) Abd El-Motaal, S. M.; Hilal, N. H.; Badawy, W. A. Stability of Zirconium Passive Films in Nitric and Sulphuric Acid Solutions. *Electrochim. Acta* 1994, 39, 2611-2617.

(12) Stephens, I. E. L.; Bondarenko, A. S.; Bech, L.; Chorkendorff, I. Oxygen Electroreduction Activity and X-Ray Photoelectron Spectroscopy of Platinum and Early Transition Metal Alloys. *ChemCatChem* 2012, 4, 341-349.
(13) Kaneko, S.; Myochi, R.; Takahashi, S.; Todoroki, N.; Wadayama, T.; Tanabe, T. Ultrahigh Vacuum Synthesis of Strain-Controlled Model Pt(111)-Shell Layers: Surface Strain and Oxygen Reduction Reaction Activity. *J. Phys. Chem. Lett.* 2017, 8, 5360-5365.
(14) Pašti, I. A.; Fako, E.; Dobrota, A. S.; López, N.; Skorodumova, N. V.; Mentus, S. V. Atomically Thin Metal Films on Foreign Substrates: From Lattice Mismatch to Electrocatalytic Activity. *ACS Catal.* 2019, 9, 3467-3481.
(15) Todoroki, N.; Kato, T.; Hayashi, T.; Takahashi, S.; Wadayama, T. Pt–Ni Nanoparticle-Stacking Thin Film: Highly Active Electrocatalysts for Oxygen Reduction Reaction. *ACS Catal.* 2015, 2209-2212.
(16) Takahashi, S.; Chiba, H.; Kato, T.; Endo, S.; Hayashi, T.; Todoroki, N.; Wadayama, T. Oxygen Reduction Reaction Activity and Structural Stability of Pt-Au Nanoparticles Prepared by Arc-Plasma Deposition. *Phys. Chem. Chem. Phys.* 2015, 17, 18638-18644.
(17) Todoroki, N.; Sasakawa, R.; Kusunoki, K.; Wadayama, T. Oxygen Reduction Reaction Activity of Nano-Flake Carbon-Deposited Pt75ni25(111) Surfaces. *Electrocatalysis* 2019, 10, 232-242.
(18) Wadayama, T.; Todoroki, N.; Yamada, Y.; Sugawara, T.; Miyamoto, K.; Iijama, Y. Oxygen Reduction Reaction Activities of Ni/Pt(111) Model Catalysts Fabricated by Molecular Beam Epitaxy. *Electrochem. Commun.* 2010, 12, 1112-1115.
(19) Dynna, M.; Marty, A. The Energetics of the Relaxation of Misfit Strain in Thin Epitaxial Films by Means of Twinning. *Acta Materialia* 1998, 46, 1087-1101.
(20) Kobayashi, S.; Wakisaka, M.; Tryk, D. A.; Iiyama, A.; Uchida, H. Effect of Alloy Composition and Crystal Face of Pt-Skin/Pt100–Xcox [(111), (100), and (110)] Single Crystal Electrodes on the Oxygen Reduction Reaction Activity. *J. Phys. Chem. C* 2017, 121, 11234-11240.
(21) Todoroki, N.; Kawamura, R.; Asano, M.; Sasakawa, R.; Takahashi, S.; Wadayama, T. Alloy-Composition-Dependent Oxygen Reduction Reaction Activity and Electrochemical Stability of Pt-Based Bimetallic Systems: A Model Electrocatalyst Study of Pt/Ptxni100−X(111). *Phys. Chem. Chem. Phys.* 2018, 20, 11994-12004.
(22) Asano, M.; Kawamura, R.; Sasakawa, R.; Todoroki, N.; Wadayama, T. Oxygen Reduction Reaction Activity for Strain-Controlled Pt-Based Model Alloy Catalysts: Surface Strains and Direct Electronic Effects Induced by Alloying Elements. *ACS Catal.* 2016, 6, 5285-5289.
(23) Zhang, J.; Vukmirovic, M. B.; Xu, Y.; Mavrikakis, M.; Adzic, R. R. Controlling the Catalytic Activity of Platinum-Monolayer Electrocatalysts for Oxygen Reduction with Different Substrates. *Angew. Chem. Int. Ed.* 2005, 44, 2132-2135.
(24) Schlapka, A.; Lischka, M.; Groß, A.; Käsberger, U.; Jakob, P. Surface Strain Versus Substrate Interaction in Heteroepitaxial Metal Layers: Pt on Ru(0001). *Phys. Rev. Lett* 2003, 91, 016101.
(25) Strasser, P.; Koh, S.; Anniyev, T.; Greeley, J.; More, K.; Yu, C.; Liu, Z.; Kaya, S.; Nordlund, D.; Ogasawara, H.; Toney, M. F.; Nilsson, A. Lattice-Strain Control of the Activity in Dealloyed Core–Shell Fuel Cell Catalysts. *Nat. Chem.* 2010, 2, 454-460.
(26) Zhang, X.; Lu, G. Computational Design of Core/Shell Nanoparticles for Oxygen Reduction Reactions. *J. Phys. Chem. Lett.* 2014, 5, 292-297.
(27) Schnur, S.; Groß, A. Strain and Coordination Effects in the Adsorption Properties of Early Transition Metals: A Density-Functional Theory Study. *Phys. Rev. B* 2010, 81, 0334021-0334024.

(28) Todoroki, N.; Asakimori, Y.; Wadayama, T. Effective Shell Layer Thickness of Platinum for Oxygen Reduction Reaction Alloy Catalysts. *Phys. Chem. Chem. Phys.* 2013, 15, 17771-17774.
(29) Yamada, Y.; Miyamoto, K.; Hayashi, T.; Iijima, Y.; Todoroki, N.; Wadayama, T. Oxygen Reduction Reaction Activities for Pt-Enriched Co/Pt(111), Co/Pt(100), and Co/Pt(110) Model Catalyst Surfaces Prepared by Molecular Beam Epitaxy. *Surf. Sci.* 2013, 607, 54-60.
(30) Todoroki, N.; Bando, Y.; Tani, Y.; Kaneko, S.; Watanabe, H.; Takahashi, S.; Wadayama, T. Communication—Electrochemical Stability of Pt/Pd(111) Model Core-Shell Structure in 80°C Perchloric Acid. *J. Electrochem. Soc.* 2017, 164, F908-F910.

Table of Contents Graphic